UC San Diego
UC San Diego Previously Published Works

Title
Measurements of 14C in ancient ice from Taylor Glacier, Antarctica constrain in situ cosmogenic 14CH4 and 14CO production rates

Permalink
https://escholarship.org/uc/item/4tr464qh

Authors
Petrenko, Vasilii V
Severinghaus, Jeffrey P
Schaefer, Hinrich
et al.

Publication Date
2016-03-01

DOI
10.1016/j.gca.2016.01.004

Peer reviewed

Measurements of ^{14}C in ancient ice from Taylor Glacier, Antarctica constrain in situ cosmogenic ^{14}CH$_4$ and ^{14}CO production rates

Vasilii V. Petrenko [a,*], Jeffrey P. Severinghaus [b], Hinrich Schaefer [c], Andrew M. Smith [d], Tanner Kuhl [e], Daniel Baggenstos [b], Quan Hua [d], Edward J. Brook [f], Paul Rose [g], Robb Kulin [e], Thomas Bauska [f], Christina Harth [b], Christo Buizert [f], Anais Orsi [b,h], Guy Emanuele [b], James E. Lee [f], Gordon Brailsford [c], Ralph Keeling [b], Ray F. Weiss [b]

[a] Department of Earth and Environmental Sciences, University of Rochester, Rochester, NY 14627, USA
[b] Scripps Institution of Oceanography (SIO), University of California, San Diego, La Jolla, CA 92093, USA
[c] National Institute of Water and Atmospheric Research Ltd (NIWA), PO Box 14901, Kilbirnie, 301 Evans Bay Parade, Wellington, New Zealand
[d] Australian Nuclear Science and Technology Organisation (ANSTO), Locked Bag 2001, Kirrawee DC, NSW 2232, Australia
[e] Ice Drilling Design and Operations, University of Wisconsin, Madison, WI, USA
[f] College of Earth, Ocean and Atmospheric Sciences, Oregon State University (OSU), Corvallis, OR 97331, USA
[g] Pristine Seas Project, National Geographic Society, 1145 17th Street N.W., Washington, D.C., USA
[h] CEA, CNRS, IPSL LSCE, F-91191 Gif Sur Yvette, France

Received 20 June 2015; accepted in revised form 10 January 2016; Available online 14 January 2016

Abstract

Carbon-14 (^{14}C) is incorporated into glacial ice by trapping of atmospheric gases as well as direct near-surface in situ cosmogenic production. ^{14}C of trapped methane (^{14}CH$_4$) is a powerful tracer for past CH$_4$ emissions from "old" carbon sources such as permafrost and marine CH$_4$ clathrates. ^{14}C in trapped carbon dioxide (^{14}CO$_2$) can be used for absolute dating of ice cores. In situ produced cosmogenic ^{14}C in carbon monoxide (^{14}CO) can potentially be used to reconstruct the past cosmic ray flux and past solar activity. Unfortunately, the trapped atmospheric and in situ cosmogenic components of ^{14}C in glacial ice are difficult to disentangle and a thorough understanding of the in situ cosmogenic component is needed in order to extract useful information from ice core ^{14}C. We analyzed very large ($\approx$1000 kg) ice samples in the 2.26–19.53 m depth range from the ablation zone of Taylor Glacier, Antarctica, to study in situ cosmogenic production of ^{14}CH$_4$ and ^{14}CO. All sampled ice is >50 ka in age, allowing for the assumption that most of the measured ^{14}C originates from recent in situ cosmogenic production as ancient ice is brought to the surface via ablation. Our results place the first constraints on cosmogenic ^{14}CH$_4$ production rates and improve on prior estimates of ^{14}CO production rates in ice. We find a constant ^{14}CH$_4$/^{14}CO production ratio (0.0076 ± 0.0003) for samples deeper than 3 m, which allows the use of ^{14}CO for correcting the ^{14}CH$_4$ signals for the in situ cosmogenic component. Our results also provide the first unambiguous confirmation of ^{14}C production by fast muons in a natural setting (ice or rock) and suggest that the ^{14}C production rates in ice commonly used in the literature may be too high.
© 2016 Elsevier Ltd. All rights reserved.

---

* Corresponding author.
  E-mail address: vpetrenk@ur.rochester.edu (V.V. Petrenko).

1. INTRODUCTION

1.1. The potential and challenges of ^{14}C in polar ice

The carbon-14 (^{14}C) content of trace gases in glacial ice is a potentially useful tracer in several paleoclimatic and geochemical applications. [14]C of methane ([14]CH_4) in ancient air is an indicator of the "fossil" ([14]C – depleted) fraction of the atmospheric methane budget (Petrenko et al., 2009). Ice core [14]CH_4 measurements can identify changes in emissions from sources such as marine methane clathrates and thawing permafrost at past times of global warming. Marine methane clathrates and permafrost have been proposed as potentially important atmospheric methane sources both for past warming events and for the future as a result of anthropogenic global warming (e.g., Kennett et al., 2000; Walter et al., 2007a,b; O'Connor et al., 2010). [14]C of CO_2 ([14]CO_2) in ice cores is potentially useful as a dating tool (Andree et al., 1984; Van de Wal et al., 1990) and could serve to improve these valuable records of past environmental change with absolute age constraints.

In addition to being trapped with C-containing atmospheric gases, ^{14}C is also produced in situ in glacial ice by cosmic rays (e.g., Lal et al., 1987). A significant fraction of this in situ cosmogenic ^{14}C appears to form carbon monoxide ([14]CO) (e.g., Lal et al., 2000; van der Kemp et al., 2002), and the in situ cosmogenic [14]CO is expected to be dominant over the trapped atmospheric [14]CO content (e.g., van Roijen et al., 1995). This potentially allows [14]CO in ice cores to be used as a tracer for the past cosmic ray flux. The solar magnetic field modulates the flux of cosmic rays (e.g., Masarik and Beer, 1999). The cosmic ray flux history reconstructed from [14]CO in polar ice cores could therefore be a useful indicator of past solar activity and potentially even solar irradiance (e.g., Steinhilber et al., 2009). Such reconstructions would require ice coring sites with well-constrained past snow accumulation rates and a thorough understanding of ^{14}C retention in the firn column (firn is the thick compacted snow layer at the top of an ice sheet; see Section 1.2).

At high geomagnetic latitudes where polar ice cores are drilled, in situ ^{14}C production rates are insensitive to variations in the geomagnetic field strength (Lal et al., 2005). This gives ice core in situ ^{14}C an important advantage over a tracer like meteoric [10]Be, which has been widely used to study past solar activity (e.g., Muscheler et al., 2007). Tracers like meteoric [10]Be, which are produced globally in the atmosphere, also have the added complication of variability in transport and deposition (e.g., Field et al., 2006). [14]C of atmospheric CO_2, which has also been used to study past cosmic ray flux and solar activity (e.g., Beer et al., 1988; Knudsen et al., 2009) suffers from uncertainties associated with temporal variations in the global carbon cycle. None of these complications are present for in situ cosmogenic ^{14}C in ice.

While it is clear that both the trapped atmospheric and in situ cosmogenic ^{14}C components in glacial ice are highly promising as geochemical tracers, they are present in a combined form and impossible to separate analytically. The in situ component of ^{14}C must be thoroughly understood before useful information can be extracted from ice core ^{14}C measurements. This understanding must include cosmogenic production rates of ^{14}C in ice and their depth dependence, the efficiency of retention of produced ^{14}C in glacial firn, the partitioning of in situ cosmogenic ^{14}C between [14]CO_2, [14]CO and [14]CH_4 and the relative magnitude of the cosmogenic ^{14}C signal as compared to the trapped atmospheric signal. Presently, our understanding of these processes is, at best, incomplete.

1.2. Polar firn and the firn-ice transition

Processes in polar firn influence the retention of in situ cosmogenic ^{14}C that is produced near the surface of ice sheets, and are relevant to some aspects of discussion of our results. We therefore provide a basic introduction to polar firn and the firn-ice transition for readers not closely familiar with ice core studies; a more comprehensive introduction can be found in Buizert et al. (2013). The top ≈50–120 m of an ice sheet are composed of compacted snow; this layer is termed the firn. The firn is sponge-like in its structure and is comprised of the ice matrix and the porosity (air-filled space). At snow accumulation zones, snow layers move downward with time through the firn column. Densification of the layers accompanies this downward movement as the porosity volume is reduced (Herron and Langway, 1980). The porosity is interconnected ("open porosity") for most of the firn thickness, allowing gases to move freely and exchange with the atmosphere, primarily by molecular diffusion (e.g., Schwander et al., 1988). As densification continues with increasing depth, a significant fraction of the air successively becomes trapped in bubbles in the ice ("closed porosity"). Eventually, some continuous impermeable ice layers form, impeding further gas diffusion and exchange with the free atmosphere (e.g., Schwander et al., 1993). This depth horizon is known as the "lock-in depth", and is typically found ≈5–15 m above the depth at which all of the air is fully sealed into bubbles and the firn zone ends.

1.3. Production, retention and partitioning of in situ cosmogenic ^{14}C in glacial ice

[14]C is produced by secondary cosmic rays from [16]O directly in the ice lattice in relatively shallow glacial ice in accumulation zones (e.g., Jull et al., 1994) as well as in ablation zones (e.g., van der Kemp et al., 2002). Confirmed production mechanisms include energetic neutrons (e.g., Lal et al., 1990) as well as negative muon capture (van der Kemp et al., 2002; Lupker et al., 2015). Production via fast muon interactions with [16]O in quartz has been demonstrated in the laboratory (Heisinger et al., 2002a) but not confirmed in a natural setting. Production of ^{14}C by thermal neutron capture from ^{14}N in air trapped in the ice has been shown to be insignificant (Buizert et al., 2012). Production rates decrease exponentially with depth for the neutron mechanism:

$$P_n(z) = P_n^0 e^{\left(\frac{-\rho z}{\Lambda_n}\right)} \tag{1}$$

where P_n^0 is the production rate at the surface (^{14}C atoms g^{-1} a^{-1}), z the depth in cm, Λ_n the neutron absorption mean free path in g cm^{-2}, and ρ the density of ice (0.92 g cm^{-3}). For the two muon mechanisms, the relationship of production rate with depth is more complex and has been formulated by Heisinger et al. (2002a, 2002b) and summarized recently by Lupker et al. (2015). Muon production rates decrease more slowly with depth than a simple exponential function. To obtain the overall ^{14}C production rate, the rates from the three individual mechanisms are summed. Surface production rates and depth dependence for each mechanism are shown in Table 1 and Fig. 1.

The hot ^{14}C atom that is produced from ^{16}O reacts to form predominantly $^{14}CO_2$ and ^{14}CO (e.g., Lal et al., 2000; van de Wal et al., 2007). Non-negligible in situ cosmogenic production of $^{14}CH_4$ was also proposed (Petrenko et al., 2009) and recently confirmed (Petrenko et al., 2013). To date, there is no agreement among prior studies on the partitioning of in situ cosmogenic ^{14}C between the different gas species. Multiple studies have included measurements of both ^{14}CO and $^{14}CO_2$, allowing for the ^{14}CO fraction of total produced ^{14}C to be examined. The results show surprisingly high variability, with estimated ^{14}CO fractions spanning almost the full 0.0–1.0 range, sometimes even within the same study (e.g., Lal et al., 2001; van de Wal et al., 2007). It may therefore be possible that the ^{14}C partitioning is different for each of the three cosmogenic production pathways.

An important additional uncertainty is related to the retention of produced in situ cosmogenic ^{14}C in glacial firn. If gases containing in situ cosmogenic ^{14}C are able to escape from the ice grains into the interconnected open porosity, they can be lost to the atmosphere. Prior studies have disagreed on the efficiency of retention of in situ ^{14}C, with measurements from some laboratories showing that a large fraction of ^{14}C is retained (e.g., Lal et al., 2000, 2001), while measurements from other laboratories showed very little or no retention of ^{14}C (e.g., Smith et al., 2000; de Jong et al., 2004; Petrenko et al., 2013). As discussed in detail in Petrenko et al. (2013), the studies that found high ^{14}C retention in firn were likely affected by procedural artifacts associated with the use of an acidified melt extraction approach. Low or no retention of in situ cosmogenic ^{14}C in firn is therefore more likely.
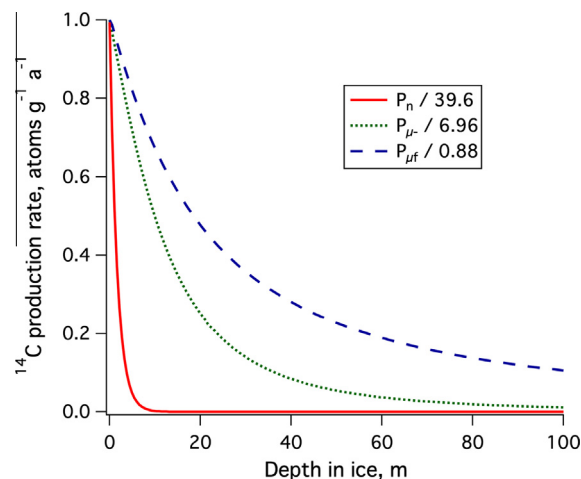

Fig. 1. Depth dependence of ^{14}C production rates in Taylor Glacier ice for the neutron (P_n), stopped negative muon ($P_{\mu-}$) and fast muon ($P_{\mu f}$) mechanisms. All production rates from Table 1 have been normalized to 1 at the surface for easier visual comparison of the depth dependence. Production by neutrons is negligible below about 10 m, while production by fast muons remains significant even at depths as large as 400 m.

1.4. Goals of this study

The study presented in this paper utilized an outcrop of ancient ($\approx$52 ka) glacial ice in the ablation zone of Taylor Glacier, Antarctica to examine the in situ cosmogenic ^{14}C content in the upper 20 m of the glacier. The relatively old age of the ice has allowed for essentially complete decay of all in situ cosmogenic or trapped atmospheric ^{14}C retained from the accumulation zone. The ^{14}C signal in this ice is therefore due mainly to in situ cosmogenic production that occurs while the ice is brought up to the surface via the process of ablation. Further, because this is solid ice, all of the in situ cosmogenic ^{14}C is quantitatively retained. Finally, the sublimation-driven ablation rates at the site have been well-characterized using stake measurements (Bliss et al., 2011). The combination of these factors allows for measurements at this site to be used to improve estimates of ^{14}C production rates and partitioning between different gas species.

Table 1
Estimates of surface total ^{14}C production rates in ice based on prior work for the neutron, negative muon capture and fast muon mechanisms. Cosmic ray flux scaling is as in Lifton et al. (2014). Production rate for neutrons is as determined by Young et al. (2014) in West Greenland for quartz, and for muons as determined by Heisinger et al. (2002b) via laboratory irradiation of quartz; the rates are transferred from quartz to ice by accounting for the number of O atoms per gram ice versus per gram quartz. We use a value of 150 g cm^{-2} for the absorption mean free path for neutrons in ice (Λ_n) (Lal et al., 1987; van de Wal et al., 2007), although we note that Nesterenok and Naidenov (2012) estimated a lower Λ_n of $\approx$130 g cm^{-2}.

Mechanism	P^0 (^{14}C atoms g^{-1} a^{-1}), sea level and high latitude	P^0 (^{14}C atoms g^{-1} a^{-1}), calculated for Taylor Glacier (elev. 527 m)
Neutrons	20.0 ± 1.5	39.6 ± 3.0
Muon capture	4.75 ± 0.4	6.96 ± 0.59
Fast muons	0.74 ± 0.4	0.88 ± 0.47

Specifically, the goals of the study were as follows:

(a) To further confirm in situ cosmogenic production of $^{14}CH_4$ using a site where a relatively large signal is expected.
(b) To provide the best estimates to date for in situ cosmogenic production rates of ^{14}CO and $^{14}CH_4$ in glacial ice.
(c) To examine the in situ cosmogenic $^{14}CH_4/^{14}CO$ ratio and explore the possibility that ^{14}CO can be used to quantify the in situ cosmogenic component of $^{14}CH_4$ in younger ice, ultimately allowing for the paleoatmospheric $^{14}CH_4$ signal to be reconstructed.

While the method used in this study for gas extraction from the ice was not optimized for quantifying $^{14}CO_2$, these measurements were still obtained and have allowed for some constraints on total ^{14}C production rates.

2. ICE SAMPLING AND ANALYTICAL METHODS

2.1. Site description

Taylor Glacier is located in the McMurdo Dry Valleys region of Antarctica (Fig. 2). Taylor Glacier ice is sourced from Taylor Dome, where a deep ice coring project has revealed the existence of >100 ka old ice (Steig et al., 2000). The very dry and windy conditions over the glacier, combined with relatively slow ice movement produce an unusually long ($\approx$80 km) ablation zone in the lower part of the glacier. Most of the ablation is via sublimation, with only the lowermost $\approx$5 km of the glacier regularly experiencing summer melt (Bliss et al., 2011). Several recent studies have examined the ice dynamics and mass balance of Taylor Glacier (Kavanaugh and Cuffey, 2009; Kavanaugh et al., 2009a,b) as well as established that ice spanning a large range of ages (Holocene to at least 130 ka) is present at the surface of the glacier (Aciego et al., 2007; Buizert et al., 2014). The ice drilling site for this study (77° 45.699′ S, 161°43.179′ E, 527 m asl; Fig. 2) is located along the center flowline of the glacier 14.0 km from the glacier terminus. The ice flow velocity at this site is $\approx$10 m/year, with an ablation rate of 0.196 ± 0.020 m/year (Bliss et al., 2011; Buizert et al., 2012).

2.2. Ice core drilling and field melt-extraction of trapped air

24-cm diameter ice cores in the 1.50–20.25 m depth range were recovered using the Blue Ice Drill from Ice Drilling Design and Operations in Madison, WI, USA (Kuhl et al., 2014). All drill components were pre-cleaned with ethanol and deionized water prior to drilling, and no drilling fluid was used. Seven complete samples were obtained, with average mid-depths of 2.26, 3.77, 5.27, 6.77, 10.02, 15.01 and 19.53 m. Each sample spanned a 1.5 m depth range. A very large amount of ice is needed for precise $^{14}CH_4$ determinations ($\approx$1000 kg, Petrenko et al., 2008a); for this reason cores for each sample were obtained from
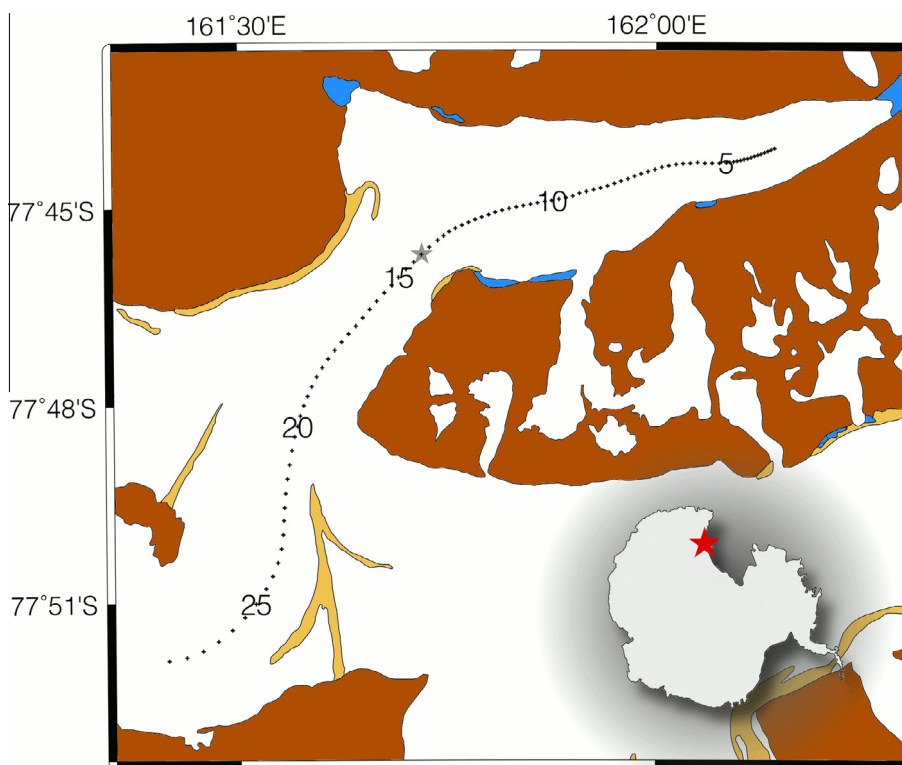

Fig. 2. Map of Taylor Glacier, showing locations of small ice samples taken along the center flowline for CH_4 and $\delta^{18}O_{atm}$ analyses during the 2009–10 season (black dots). Numbers denote distance in km from glacier terminus. Gray star shows the location of the $\approx$52 ka ice used in this study. Inset shows Taylor Glacier location in Antarctica.

21 parallel boreholes. These boreholes were located along the center flow-line of the glacier with an average spacing of 0.87 m between the boreholes. In preparation for on-site gas extraction, the ice cores were cleaned by scraping all surfaces with electropolished stainless steel chisels.

Ice cores were melted on-site to extract the trapped gases using the large-volume clean sampling apparatus ("melter") described in Petrenko et al. (2008a, 2013). Modifications from the gas extraction procedure described in Petrenko et al. (2013) were as follows. During the melter headspace flush-evacuation sequence (prior to ice melting), ultrapure air ([CH$_4$] < 10 ppb, [CO] < 10 ppb, [CO$_2$] < 1 ppm) was used instead of ultrapure N$_2$ and Ar, and the flush was done 3 times. After the final flush, the ice melter headspace was evacuated for 15 min after the pressure reached a value 1 torr above the expected vapor pressure over ice. Unlike in the Petrenko et al. (2013) firn study, no carrier gas was needed with Taylor Glacier ice; instead, the air trapped in the ice cores served as the carrier for in situ cosmogenic ^{14}C. The gas recirculation step (needed to equilibrate the in situ cosmogenic ^{14}C between the melt water and head-space) was 30 min long. On average, 386 kg of ice per melt-extraction was used, and air from 3 melt-extractions was combined into a single sample.

The 30 min duration of the recirculation step (to allow for equilibration of trace gases between the water and the headspace) was established at the start of the field season as follows. Melt water from a sample extraction was purged with ultrapure air, and the headspace was evacuated. One of the standard gases was introduced into the headspace (to a pressure mimicking a sample extraction), and the recirculation of gas through the bubbler was started. At five-minute intervals, an aliquot of the gas was analyzed for CO$_2$ mole fraction ([CO$_2$]) using a LI-820 infrared CO$_2$ analyzer from LI-COR® Biosciences (Fig. S1a in the Electronic Annex). The time needed until [CO$_2$] was no longer appreciably changing was set as the procedural recir-culation time. To further test that gas equilibration time is the same when the gas is initially dissolved in the water (which may be the case for in situ cosmogenic ^{14}C), the headspace was again evacuated, and ultrapure air was introduced. The recirculation was started again, and the gradual evasion of CO$_2$ from the water into the headspace was monitored, confirming that 30 min was again sufficient (Fig. S1b).

In an attempt to obtain a better characterization of in situ cosmogenic ^{14}CO$_2$, we measured pH of the melt water following the gas extraction. This measurement, com-bined with the known [CO$_2$] in the headspace in principle allows for quantification of the total amount of inorganic carbon in the system (CO$_2$ gas, dissolved CO$_2$, bicarbonate ion (HCO$_3^-$) and carbonate ion (CO$_3^{2-}$)). Following the transfer of sample air from the melter headspace into storage canisters, the melter headspace was vented with CO$_2$-free air to avoid interference of atmospheric CO$_2$ with the pH measurement. pH measurements were made inside a box flushed with CO$_2$-free air, with the melt water plumbed directly into this box. An Orion™ ROSS Ultra™ Triode™ was used for the measurement, in combination with a set of low ionic strength buffers for electrode calibration as well as an ionic strength adjustor solution for pure water. Approximately 1 L of melt water was flushed through the tubing prior to taking the pH sample aliquots, and the mea-surement was done in triplicate on separate aliquots of melt water.

2.3. Tests of melt-extraction procedural effects

Two types of procedural tests on the large-volume gas melt-extraction system were conducted to investigate effects of added extraneous carbon on measured ^{14}CH$_4$ in the sam-ples. As previously described for this system (Petrenko et al., 2008a, 2013), tests involving introducing standard gases over the melt water from sample ice were conducted in the field. For this study, two different standard gases were used. Both gases contained ≈490 ppb of CH$_4$, to mimic the average CH$_4$ mole fraction ([CH$_4$]) expected in the sampled ice. One of the gases contained CH$_4$ derived from a fossil source and expected to be essentially free of ^{14}C ("^{14}C-dead standard"), while the other gas ("^{14}C-modern standard") contained modern atmospheric CH$_4$ (from Niwot Ridge, CO, USA), with an expected ^{14}C activity of ≈130 percent modern carbon (pMC; as defined in Stuiver and Polach (1977)). Both gases also contained CO$_2$ (≈215 ppm) and CO (≈85 ppb) to mimic the expected levels in the sample ice. The gases also contained ≈100 ppm each of Kr and Xe, for use as tracers of gas partitioning between the melt water and the head-space in the ice melter (Petrenko et al., 2013). The pH measurements described above were also performed on the melt water following the field procedural tests.

Using two standard gases with distinct ^{14}CH$_4$ activities allows for complete characterization of both the mass and ^{14}C activity of extraneous carbon added during sample pro-cessing. The air samples derived from these field procedural tests undergo treatment identical to that of air derived from the actual ice samples, allowing the tests to characterize extraneous carbon from all steps of sample processing.

As described by Petrenko et al. (2013), the field procedu-ral tests successfully mimic all aspects of sample processing except for the ice melting step. The melting step results in heating of the walls of the aluminum melt-extraction cham-ber (up to 50 °C) and potentially increased outgassing of CH$_4$. For this reason, additional procedural tests were con-ducted at SIO to specifically investigate the effects of ice melting. More than 2000 kg of gas-free ice was obtained from a commercial supplier that provides clear ice blocks for carving ice sculptures. Very slow uni-directional freez-ing of this ice over several days allows for all gases to be excluded from the ice lattice. 16 sub-samples of this gas-free ice were analyzed for [CH$_4$] at OSU using the usual "blank" ice procedure (Mitchell et al., 2013); these analyses revealed no differences between this ice and gas-free ice rou-tinely made at the OSU laboratory, confirming that no sig-nificant amount of CH$_4$ was present. The standard gases described above were used to provide the air during simu-lated melt extractions with this gas-free ice, with the gas being introduced just before the start of the melting step. One complete test sample was collected using the ^{14}C-dead standard, and another test sample using the

^{14}C-modern standard; as in the field, each sample was comprised of 3 melt-extractions. To ensure the most direct assessment of procedural effects from the ice-melting step, further over-water procedural tests were conducted at SIO immediately following the gas-free ice tests.

All of the over-water procedural tests included a water purging step prior to each simulated extraction, in which ultrapure air ($[CH_4] < 10$ ppb) was introduced into the melter via a bubbler manifold at the bottom (Petrenko et al., 2013) and evacuated from the headspace via the top. The progress of the purge was monitored by directing part of the evacuated airstream through a cryogenic drying trap into the LI-820 CO_2 analyzer. The purge was conducted until measured CO_2 reached the baseline value determined by flowing the ultrapure air directly into transfer lines and pumps, bypassing the melter itself. Fig. S1c in the Electronic Annex shows the typical time evolution of CO_2 in air being pumped from the melter headspace during a purge.

Because the amount of in situ cosmogenic ^{14}CO in sampled ice was expected to be very large relative to any ^{14}CO addition from the melt-extraction procedure, no tests to quantify such procedural ^{14}CO addition were conducted.

2.4. Laboratory analyses and sample processing

Air samples and procedural tests were first analyzed at SIO for $[CH_4]$ by a gas chromatograph (GC) with a flame ionization detector (FID), as well as for CFC-11, CFC-12 and SF_6 (to constrain inclusion of modern ambient air) by GC–mass spectrometry (GC–MS) (Mühle et al., 2007). The procedural tests were further analyzed for $\delta(Xe/N_2)$ and $\delta(Kr/N_2)$ (Thermo MAT 253 isotope ratio MS (IRMS)) at SIO. CO_2 for subsequent ^{14}C analyses was extracted at SIO from ≈ 1 standard liter (SL) of air for all samples, field procedural tests and standard gases (Leuker, 1998).

$[CO]$ and $[CO_2]$ in the samples, procedural tests, and standard gases were analyzed at NIWA using a GC setup as described by Lowe et al. (1991) with a reducing gas detector and a methanizer-FID, respectively. $\delta^{13}CH_4$ in the samples was analyzed by a continuous-flow method at NIWA using an IsoPrime IRMS (Ferretti et al., 2005), with a correction applied for krypton interference following Schmitt et al. (2013). $\delta^{13}CH_4$ in the standard gases was analyzed by dual-inlet on a MAT 252 IRMS as described in Petrenko et al. (2008b).

The air in the samples, procedural tests and standard gases was then processed to oxidize CH_4 to CO_2; this CO_2 was captured for further handling, as described in Petrenko et al. (2008b, 2009). Unfortunately, one of the $^{14}CH_4$ samples (5.27 m) was lost at this stage due to a problem with flame-sealing of sample CO_2 into a Pyrex tube. ≈ 20 SL of air was retained in each sample canister for ^{14}CO analyses, and this remaining air was diluted with a gas containing 10.23 ppm of ^{14}C-depleted CO in ultrapure air to increase carbon mass for ^{14}CO measurements. $\delta^{13}CO$ in this high-$[CO]$ gas was determined at NIWA following Brenninkmeijer (1993). After the dilution, the samples were processed to oxidize CO to CO_2; this CO_2 was captured for further handling, as described in Petrenko et al. (2008b, 2009).

The resulting pure CO_2 samples (derived from CO_2, CO or CH_4) were converted to graphite by using an excess of H_2 over a Fe catalyst in the conventional graphitization lines at ANSTO (Hua et al., 2004). We used Sigma–Aldrich Fe_2O_3 (mesh size unspecified, 99.999% purity). Before the graphitization, the iron oxide was reduced to Fe by reaction with ≈ 750 mbar pure H_2 at 600 °C for 1 h. By-product water vapor produced during the graphitization was efficiently trapped using a cold finger system at -80 °C (Yang et al., 2013). Typical graphitization efficiency was high: $\approx 90\%$ for 20 µg C samples and $\approx 100\%$ for 70–100 µg C samples. Unfortunately, one further $^{14}CH_4$ sample (10.02 m) was lost at this stage while extracting sample CO_2 from the sealed Pyrex tube. Graphite derived from all samples, procedural tests and standard gases was subsequently measured for ^{14}C by AMS on the 10 MV ANTARES accelerator at ANSTO (Fink et al., 2004). The final sample sizes (determined prior to graphitization) were ≈ 55 µg C for $^{14}CO_2$, ≈ 20 µg C for $^{14}CH_4$ and ≈ 85 µg C for ^{14}CO.

3. RESULTS

The in-situ cosmogenic ^{14}C content in ice for the gas species X can be calculated as (see the Electronic Annex for a derivation):

$$^{14}C_X = \frac{pMC}{100} \times e^{-\lambda(y-1950)} \times \frac{\left(1+\frac{\delta^{13}C_X}{1000}\right)^2}{0.975^2}$$
$$\times 1.1694 \times 10^{-12} \times [X] \times Air \times \frac{1}{1000} \times \frac{1}{22.4} \times N_A \qquad (2)$$

where $^{14}C_X$ is the number of ^{14}C-bearing molecules of gas X per gram of ice, pMC is the ^{14}C activity of the gas after all corrections, λ is the ^{14}C decay constant (1.216×10^{-4} a^{-1}), y is the year of measurement, $\delta^{13}C_X$ is the $\delta^{13}C$ of the gas, 0.975 is a factor arising from ^{14}C activity normalization to $\delta^{13}C$ of -25‰ (part of definition of pMC (Stuiver and Polach, 1977)), 1.1694×10^{-12} is the $^{14}C/(^{13}C + ^{12}C)$ ratio corresponding to the absolute international standard activity (AISA) (Hippe and Lifton, 2014), $[X]$ is the gas molar fraction in extracted air after all corrections, Air is the air content of the ice in cc STP g^{-1}, 22.4 is the number of STP liters of gas per mole, and N_A is the Avogadro constant.

The ^{14}C activity as well as the gas molar fraction measured in the samples can be altered by addition of extraneous carbon at various stages of processing. These procedural effects must be quantified and corrected for before the true ^{14}C content of the ice can be determined. Detailed discussion of the corrections for all gas species as well as of the determination of the air content is presented in the Electronic Annex. Briefly, all reported uncertainties are 1 σ unless otherwise specified, and uncertainties for calculated quantities are determined by standard error propagation techniques. Sample $[CH_4]$ and $^{14}CH_4$ were corrected for the effects of (a) gas dissolution in the melter, (b) overall procedural effects based on procedural test results, (c) a small amount of additional CH_4 produced during the melting step and (d) inclusion of a small amount of ambient air via fractures in the shallowest samples. Measured $[CH_4]$ and $^{14}CH_4$ values as well as values after

all corrections and the calculated $^{14}CH_4$ content in the ice are presented in Table 2 and Fig. 3.

Sample [CO] and ^{14}CO were corrected for the effects of (a) dilution with the high-[CO], ^{14}C-depleted gas, (b) in situ cosmogenic production of ^{14}CO in the sample canisters during transport and storage, (c) CO added during the melt-extraction and sample storage and (d) gas dissolution in the melter. Measured ^{14}CO values and the ^{14}CO content

Table 2
Sample [CH₄] and $^{14}CH_4$ as measured and after all procedural corrections, as well as calculated ice $^{14}CH_4$ content. All [CH₄] values are reported on the Tohoku University scale (Cunnold et al., 2002). Note that the effect of ^{14}C corrections is largest for the shallowest 2 samples which are affected by ambient air inclusion via fractures in the ice.

| Sample mid-depth, m	Measured [CH₄], ppb	[CH₄] after all corrections, ppb	Measured $^{14}CH_4$, pMC	$^{14}CH_4$ after all corrections, pMC	Ice $^{14}CH_4$ content, molecules/g
2.26	468.8 ± 0.3	461.6 ± 4.9	33.2 ± 0.3	29.9 ± 1.6	0.418 ± 0.026
3.77	473.5 ± 0.2	476.1 ± 2.4	24.2 ± 0.3	22.8 ± 0.8	0.327 ± 0.013
5.27	485.8 ± 0.2	492.0 ± 6.1	Sample lost		
6.77	493.0 ± 0.2	502.7 ± 2.0	17.4 ± 0.2	17.4 ± 0.5	0.273 ± 0.010
10.02	515.9 ± 0.4	525.4 ± 2.0	Sample lost		
15.01	518.7 ± 0.2	528.6 ± 2.0	13.9 ± 0.2	13.7 ± 0.5	0.206 ± 0.008
19.53	531.4 ± 0.3	541.6 ± 2.0	13.0 ± 0.2	12.8 ± 0.5	0.182 ± 0.008
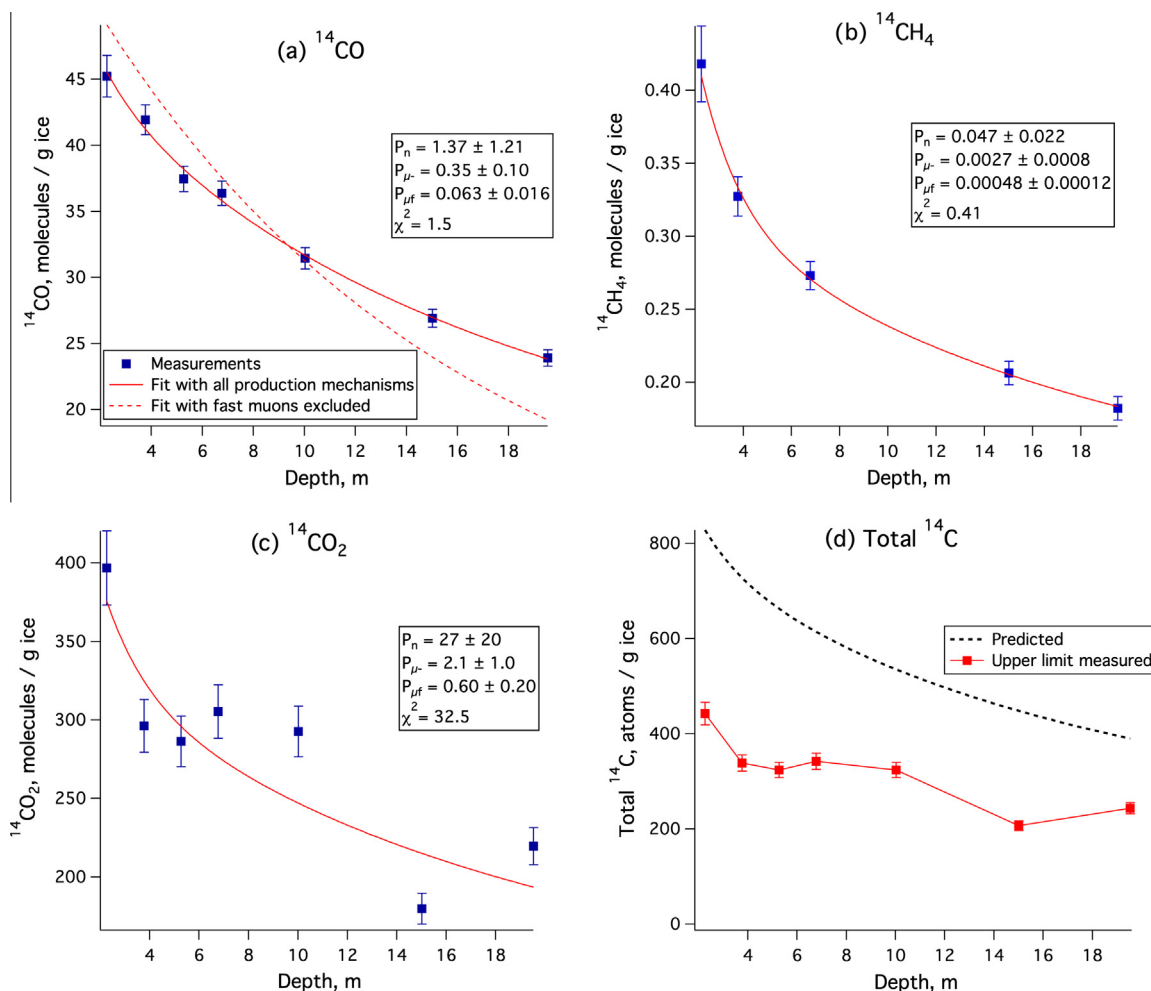
Fig. 3. (a) ^{14}CO content after all corrections (markers) and least-squares fit lines as described in the text. All production rate estimates are for Taylor Glacier site ice surface (^{14}C atoms g^{-1} a^{-1}). χ^2 value for the quality of "all mechanisms" fit is also shown. The best fit with fast muons excluded had $\chi^2 = 190$. Uncertainties for P_n, $P_{\mu-}$ and $P_{\mu f}$ incorporate contributions from the curve fit, ablation rate and depth of long-term transport. (b) Similar to (a), but for $^{14}CH_4$. Uncertainties for $P_{\mu-}$ and $P_{\mu f}$ are propagated from corresponding uncertainties for ^{14}CO production rates and $^{14}CH_4/^{14}CO$ ratio. (c) Similar to (a) and (b), but for upper limit of $^{14}CO_2$ content in the ice. (d) Upper limit of total ^{14}C measured in the ice and predicted total ^{14}C. Predicted ^{14}C is determined by using cumulative ^{14}C formulations as described in Section 4.4 and the Electronic Annex, and surface production rates as in Table 1.

Table 3
^{14}CO activities measured in the samples and final calculated ice ^{14}CO content.

Sample mid-depth, m	Measured ^{14}CO, pMC	Ice ^{14}CO content, molecules/g
2.26	126.9 ± 0.6	45.2 ± 1.6
3.77	121.7 ± 0.6	41.9 ± 1.1
5.27	96.2 ± 0.5	37.5 ± 1.0
6.77	91.7 ± 0.5	36.4 ± 0.9
10.02	81.3 ± 0.4	31.4 ± 0.8
15.01	79.5 ± 0.4	26.9 ± 0.7
19.53	75.3 ± 0.5	23.9 ± 0.6

Table 4
Measured $^{14}CO_2$ activities in the samples, as well as estimated maximum $^{14}CO_2$ content in the ice. $^{14}CO_2$ activities have not been normalized for $\delta^{13}C$, as $\delta^{13}C$ was not measured. Since other uncertainties associated with the $^{14}CO_2$ determination are relatively large, the lack of $\delta^{13}C$ values results in a negligible increase in the overall uncertainty ($\approx 0.25\%$ relative uncertainty increase).

Sample mid-depth, m	Measured $^{14}CO_2$, pMC	Upper limit of $^{14}CO_2$ in sampled ice, molecules/g
2.26	41.6 ± 0.4	397 ± 24
3.77	32.7 ± 0.3	296 ± 17
5.27	30.0 ± 0.4	286 ± 16
6.77	31.2 ± 0.3	305 ± 17
10.02	30.3 ± 0.4	293 ± 16
15.01	21.7 ± 0.3	180 ± 10
19.53	25.8 ± 0.3	220 ± 12

in the ice calculated after all corrections are shown in Table 3 and Fig. 3.

We consider the $^{14}CO_2$ analyses and results somewhat speculative because of problems and uncertainties inherent in the melt-extraction approach. However, these results do add some useful information to the discussion and were therefore included. We were only able to constrain the upper limit of $^{14}CO_2$ present in the ice; see the Electronic Annex for a detailed discussion. Table 4 and Fig. 3 show the measured $^{14}CO_2$ activities as well as estimated maximum ice $^{14}CO_2$ content.

4. DISCUSSION

4.1. Comparison with prior ice cosmogenic ^{14}C data quality and measurement methods

Our method is currently the only one capable of $^{14}CH_4$ measurements in ice, because it accommodates the very large sample size requirement. In the one prior study of in situ cosmogenic $^{14}CH_4$ (at Summit, Greenland; Petrenko et al., 2013) the average relative error on $^{14}CH_4$ determinations was 13%, while in the present work it is 4%. Most of the improvement has resulted from larger $^{14}CH_4$ content in Taylor Glacier ice compared to Greenland Summit firn, with additional improvements from better determinations of effective air content in the ice as well as of procedural ^{14}C effects.

The ^{14}CO determinations were also improved as compared to Petrenko et al. (2013); with a reduction in relative error from 22% to 2.6%. In this case, most of the improvement arises from better-constrained dilution with ^{14}C-depleted CO, with additional improvement due to larger ^{14}CO content in the ice. In comparison with the best prior work that determined ^{14}CO in ablation zone ice samples with similar ^{14}CO content (van der Kemp et al., 2002), our errors are an order of magnitude lower. This is mainly due to the much larger sample size used in our work.

Petrenko et al. (2013) provided a detailed discussion of the general advantages of our approach for in situ cosmogenic $^{14}CH_4$ and ^{14}CO determinations as compared to most prior work; we summarize these briefly here. First, our air extractions are performed in the field immediately after core recovery, eliminating the uncertainties associated with non-negligible additional ^{14}C production during ice core transport and storage. Second, melt-extraction combined with water – headspace gas equilibration ensures complete recovery of ^{14}C from ice grains, which may be a problem with dry-extraction methods. Finally, our method includes very thorough characterization of procedural ^{14}C effects for all parts of sample processing.

Our method performed poorly for $^{14}CO_2$ because melt-extraction techniques inherently lead to artifacts in CO_2 (see Electronic Annex for detailed discussion). However, our $^{14}CO_2$ results are likely more reliable than the majority of prior work that used the melt-extraction approach (Lal et al., 1990, 1997, 2000, 2001; Jull et al., 1994). As discussed in detail in Petrenko et al. (2013), the use of acid in those prior studies combined with inadequate procedural blank characterization likely resulted in addition of considerable extraneous ^{14}C. Of the in situ cosmogenic $^{14}CO_2$ studies available to date, we consider the studies done by dry extraction (e.g., Smith et al., 2000; van de Wal et al., 2007) to be more reliable than any melt-extraction approaches, including our own. However, even results from those studies harbor unknown uncertainties from $^{14}CO_2$ production during ice core transport and storage, as well as from possibly incomplete release of in situ cosmogenic $^{14}CO_2$ from ice grains during the extraction.

4.2. Possible contribution of ^{14}C from the accumulation zone

As discussed in Sections 1.1 and 1.3, accumulation-zone ice can acquire ^{14}C via both trapping of atmospheric gases and in situ cosmogenic production. To assess whether the sampled ice has any remnant signal of ^{14}C from the accumulation zone, both the age of the ice and the possible cumulative in situ cosmogenic ^{14}C production at the accumulation site need to be constrained.

Prior work on Taylor Glacier used measurements of δD of ice to establish a preliminary age scale for ice outcropping along the center flowline shown in Fig. 2 (Aciego et al., 2007). Further samples collected along the center flowline during the 2009–10 Antarctic season added constraints based on $[CH_4]$ and the isotopic composition of atmospheric O_2 ($\delta^{18}O_{atm}$) (Baggenstos, 2015). The oldest unambiguously dated ice (≈ 52 ka) identified based on the preliminary analysis of the 2009–10 results was at 14 km

from the glacier terminus (Fig. 2); this was the location chosen for our in situ cosmogenic ^{14}C study. The center flowline sample taken at 5 m depth at this location yielded an average $\delta^{18}O_{atm}$ value of 0.247‰ and a [CH$_4$] value of 492 ppb (Fig. 4). Such a $\delta^{18}O_{atm}$ value is plausible for gas ages of at least 49–56 ka (Severinghaus et al., 2009). The only younger period when such a $\delta^{18}O_{atm}$ value occurs is during the Preboreal between 10 and 11 ka, but the Preboreal is associated with [CH$_4$] > 600 ppb. The [CH$_4$] values contained in this low-$\delta^{18}O_{atm}$ section of the TG profile (14.0 km: 492 ppb; 13.7 km: 522 ppb; 13.4 km: 557 ppb; Fig. 4) are also indicative of a Dansgaard–Oeschger type [CH$_4$] oscillation. Such an oscillation is present in Antarctic ice cores at 50–55 ka (Brook et al., 2005; WAIS Divide Project Members, 2015). The [CO$_2$] value of 212 ppm measured in the 14.0 km sample is also consistent with a gas age of 52–55 ka (Ahn and Brook, 2008). We cannot identify another time interval during the last glacial when the same combination of values for these 3 tracers re-occurs. Finally, the age we infer is in agreement with the age obtained through ^{81}Kr radiometric dating of ice at this location, which suggested an age of 46 ± 21 ka (Buizert et al., 2014).

Sample age increases with depth at most sampled locations on Taylor Glacier (Baggenstos, 2015), including at our ^{14}C sampling site. On Fig. 4, the [CH$_4$] trend measured in the large-volume samples was visually matched to the high-resolution [CH$_4$] record from the WAIS Divide ice core (WAIS Divide Project Members, 2015) to arrive at sample gas age estimates. The 2.26 m (youngest) sample has an estimated age of 50.4 ka, while the 19.53 m (oldest) sample has an estimated age of 53.4 ka. After 50.4 ka of decay, the remaining $^{14}CO_2$, ^{14}CO and $^{14}CH_4$ from trapped air are much smaller than the respective uncertainties on our measurements and can be ignored. Given the large age of the samples, we also assume that we can ignore the contribution from in situ cosmogenic ^{14}C produced in the accumulation zone. We test this assumption in Section 4.4, finding it to be valid.

4.3. $^{14}CH_4$ and $^{14}CH_4/^{14}CO$ ratio

The values for $^{14}CH_4$ content (Table 2) in the ice provide further confirmation that in situ cosmogenic production of $^{14}CH_4$ takes place. This confirmation is stronger in the present study than in the earlier Petrenko et al. (2013) work, with more samples and higher measured $^{14}CH_4$.

Table 5 shows the $^{14}CH_4/^{14}CO$ ratio. As can be seen, this ratio appears to be effectively constant for all except the shallowest (2.26 m) sample. As Table 5 also shows, expected ^{14}C contribution from the neutron mechanism is relatively small or negligible for all except the 2.26 m sample. ^{14}C fraction from negative muon capture is relatively constant and represents the largest component at all depths, while the contribution from fast muons grows steadily with
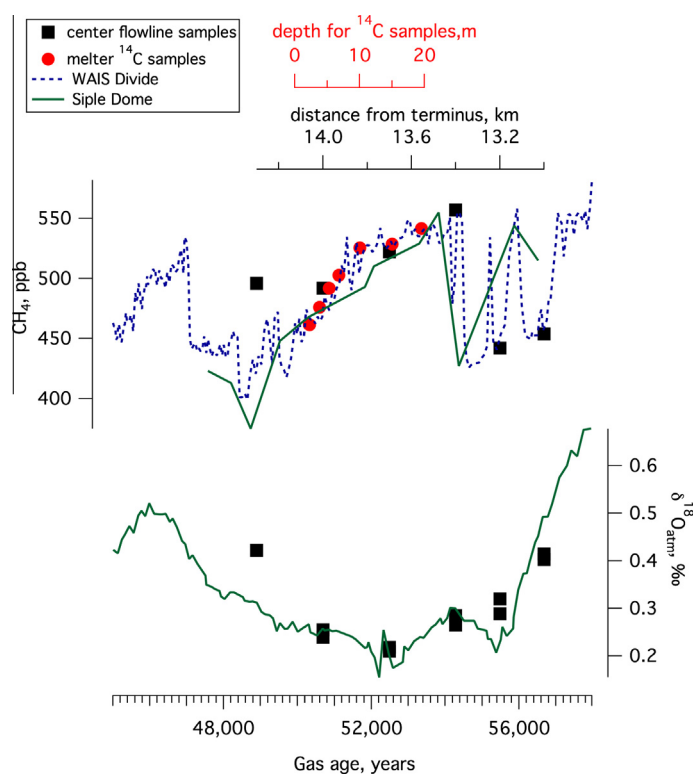

Fig. 4. Data used to constrain the gas age of the large-volume samples used for ^{14}C analyses. Siple Dome [CH$_4$] is from Brook et al. (2005). WAIS Divide ice core [CH$_4$] is from Buizert et al. (2015) and WAIS Divide Project Members (2015). Siple Dome ice core $\delta^{18}O_{atm}$ data are from Severinghaus et al. (2009). Note that neither the distance-age relationship for the center flowline samples, nor the depth-age relationship for the ^{14}C samples is expected to be linear; this likely causes the mismatches in [CH$_4$] and $\delta^{18}O_{atm}$ outside the 50–55 ka age range of main interest.

Table 5
Measured $^{14}CH_4/^{14}CO$ ratio for finalized ice ^{14}C content, and the fraction of expected total ^{14}C attributable to each production mechanism. Expected fractions were calculated using Taylor Glacier surface production rates as in Table 1 and depth-production rate formulations as described in Section 4.4 and the Electronic Annex.

Sample mid-depth, m	$^{14}CH_4/^{14}CO$ ratio	Expected fraction of ^{14}C from neutrons	Expected fraction of ^{14}C from muon capture	Expected fraction of ^{14}C from fast muons
2.26	0.0092 ± 0.0005	0.10	0.61	0.29
3.77	0.0078 ± 0.0003	0.05	0.63	0.33
5.27		0.02	0.63	0.35
6.77	0.0075 ± 0.0003	0.01	0.62	0.37
10.02		0.00	0.59	0.40
15.01	0.0077 ± 0.0003	0.00	0.55	0.45
19.53	0.0076 ± 0.0003	0.00	0.51	0.49

increasing depth. The expected ratio between ^{14}C from negative muons and ^{14}C from fast muons decreases from 1.9 at 3.77 m to 1.0 at 19.53 m. The constant $^{14}CH_4/^{14}CO$ ratio in this entire depth range suggests that this ratio (0.0076 ± 0.0003) is the same for both muon ^{14}C production mechanisms.

The significantly higher $^{14}CH_4/^{14}CO$ ratio for the 2.26 m sample suggests that the ^{14}C partitioning is different for the neutron production mechanism, resulting in relatively more $^{14}CH_4$. Due to the relatively small overall ^{14}C contribution from neutrons, our data leave the neutron $^{14}CH_4/^{14}CO$ production ratio poorly constrained (see Fig. 3). We note, however, that a relatively higher $^{14}CH_4/^{14}CO$ production ratio for neutrons than for muons is qualitatively consistent with the value observed in shallow Greenland firn by Petrenko et al. (2013) (0.021 ± 0.005 for Sample 1, which was considered to be the most reliable of the three $^{14}CH_4$ determinations). For the firn samples in the Petrenko et al. (2013) study, 95% of all in situ cosmogenic ^{14}C was expected to be from the neutron production mechanism.

The constant $^{14}CH_4/^{14}CO$ ratio for both muon production mechanisms means that the in situ cosmogenic component of $^{14}CH_4$ can be accurately determined based on measured ^{14}CO in ice that does not contain significant neutron-produced ^{14}C. This cosmogenic component could then be corrected for, allowing for accurate reconstructions of paleoatmospheric $^{14}CH_4$. The trapped atmospheric component of ^{14}CO is negligibly small in comparison to ^{14}CO from in situ cosmogenic production. For example, we calculate that trapped air from the Younger Dryas–Preboreal climate transition at 11.5 ka would contain only 0.3 ^{14}CO molecules per gram of ice, or about 100 times less than what is observed due to ablation-zone in situ cosmogenic production in Taylor Glacier ice at 10 m depth.

In addition to ablation-zone production, ice with ages much younger than 50 ka would also contain significant ^{14}C from in situ cosmogenic production in the accumulation zone. However, this ^{14}C would begin accumulating starting only at the lock-in depth (see Section 1.2) where the first impermeable ice layers begin to form, and gas exchange with the atmosphere and the upper part of the firn effectively stops (e.g., Schwander et al., 1993). The lack of in situ cosmogenic ^{14}C accumulation above the lock-in depth is supported by the results of our recent firn ^{14}C study at Summit, Greenland (Petrenko et al., 2013), as well as by

results of most other studies (e.g., van der Kemp et al., 2000; de Jong et al., 2004) that avoided the problematic melt-acidify air extraction approach. At the lock-in depth (typically >25 m solid ice equivalent), ^{14}C production from the shallow-penetrating neutron mechanism is minimal or non-existent. It can therefore be assumed that effectively all of the in situ cosmogenic ^{14}C in sampled ice at Taylor Glacier (if taken below $\approx$5 m in ablating ice) is from the muon production mechanisms. The determined $^{14}CH_4/^{14}CO$ ratio could then be applied to make the correction for in situ cosmogenic $^{14}CH_4$.

4.4. Discussion of observed ^{14}C production rates

Fig. 3 shows the $^{14}CH_4$ and ^{14}CO content in sampled ice after all corrections, as well as the upper limit of the $^{14}CO_2$ and total ^{14}C content. We use these results to estimate surface ^{14}C production rates for each species by each mechanism. This is accomplished via a least-squares curve fit to the data using an expression that describes cumulative ^{14}C as a function of depth. The expression used for cumulative ^{14}C is described in full detail in the Electronic Annex; here we provide a more abbreviated discussion. For the neutron mechanism, an exponential depth dependence of production rate is assumed (Eq. (1)), using a value of 150 g cm^{-2} for the mean free path Λ_n (Lal et al., 1987; van de Wal et al., 2007). Integrated over depth, this yields the following for cumulative ^{14}C from neutrons (Lal et al., 1990):

$$^{14}C_n(z) = \frac{P_n^0 e^{-\rho z/\Lambda_n}}{\frac{\rho A}{\Lambda_n} + \lambda} \tag{3}$$

where A is the ice ablation rate (in cm a^{-1}) and other terms are as previously defined.

For the muon mechanisms, we use the depth dependence as formulated by Heisinger et al. (2002a, 2002b) and summarized recently by Lupker et al. (2015). For the purpose of curve fitting, we successfully approximate the depth dependence for negative muon capture with a 2-term exponential, and with a 3-term exponential for fast muons (Fig. S2 in Electronic Annex). For negative muon capture, integrating over depth yields an expression for cumulative ^{14}C that has 2 exponential terms equivalent in form to Eq. (3).

The expression for cumulative ^{14}C from fast muons is slightly more complex because, unlike for neutrons and negative muon capture, there is non-negligible ^{14}C production during long-term ice transport at large depths. Ice flow modeling suggests that our sampled ice travels at a depth of $\approx$300–500 m through much of the length of Taylor Glacier (Buizert et al., 2012). In this case, the cumulative ^{14}C from fast muon production (whose depth dependence is approximated by a 3-term exponential) is given by:

$$^{14}C_{\mu f}(z) = De^{\lambda z/A}$$
$$+ P_{\mu f}^0 \left(\frac{f_{\mu f1}e^{-\rho z/\Lambda_{\mu f1}}}{\frac{\rho A}{\Lambda_{\mu f1}} + \lambda} + \frac{f_{\mu f2}e^{-\rho z/\Lambda_{\mu f2}}}{\frac{\rho A}{\Lambda_{\mu f2}} + \lambda} + \frac{f_{\mu f3}e^{-\rho z/\Lambda_{\mu f3}}}{\frac{\rho A}{\Lambda_{\mu f3}} + \lambda} \right)$$
$$(4)$$

The Λ's represent the effective absorption mean free path for each exponential term and the f's represent the fractional contribution of each term to the total production rate at the surface. D is a constant (in ^{14}C atoms/g) that is related to the ^{14}C content at a reference depth z_{deep}. For the case of long-term transport at z_{deep}, it can be shown that D is directly proportional to the surface production rate $P_{\mu f}^0$ (see Electronic Annex). In the resulting expression for cumulative ^{14}C from all mechanisms as a function of depth, each of the 7 exponential terms is proportional to one of the surface production rates (P_n^0, $P_{\mu-}^0$, or $P_{\mu f}^0$) and the three production rates are the only free parameters that are determined by the least-squares curve fit.

One major source of uncertainty in determining surface ^{14}C production rates from our data is the choice of average depth for long-term ice transport between the accumulation zone and our ablation site. This mainly affects $P_{\mu f}^0$. For the purposes of curve fitting, we assume 400 m for the average depth of long-term transport. We incorporate the uncertainty in this depth by also running scenarios where the average depth of transport is as shallow as 300 m or as deep as 500 m ($P_{\mu f}$ is 3× greater at 300 m than at 500 m), and including the full range of resulting $P_{\mu f}^0$ values in the reported error.

Another major source of uncertainty in determining surface ^{14}C production rates from our data is the ice ablation rate. Ablation stake measurements yield 0.196 ± 0.020 m a^{-1} for the sampled part of the glacier (Bliss et al., 2011; Buizert et al., 2012). However, the ablation stakes represent at most 8 years of measurements (2002–2010), whereas longer-term rates are needed for the cumulative ^{14}C calculations. If we consider that the ice rises from a depth of $\approx$400 m, then the last $\approx$2000 years are in principle of interest, although ablation rate variations become less important further back in time due to lower production rates at greater depths.

Stronger winds and warmer temperatures result in faster ablation rates on Taylor Glacier, with katabatic wind speed being the dominant variable for much of the glacier length (Bliss et al., 2011). A weather record from nearby McMurdo Sound suggests that 2002–2010 was 0.4 °C warmer than 1957–2003 (National Climatic Data Center,

2015). It is likely that the Dry Valleys – McMurdo Sound area was $\approx$2 °C cooler and experienced somewhat stronger katabatic winds during the Little Ice Age (Bertler et al., 2011; Rhodes et al., 2012). It is also possible that, during the initial phase of its ascent from 400 m to the surface, sampled ice was traveling in a zone with higher ablation rates of $\approx$0.25 m a^{-1} (Buizert et al., 2012). To account for all these factors, we use a doubled uncertainty of ±0.04 m a^{-1} for the long-term ablation rate. We used curve fit scenarios that span the full range of possible ablation rates to estimate the corresponding contribution to uncertainties in surface production rates.

Our data provide better constraints for production rates for ^{14}CO than for ^{14}CH$_4$, due to the larger number of ^{14}CO data points. P_n^0, $P_{\mu-}^0$ and $P_{\mu f}^0$ for ^{14}CO were all determined by a least-squares curve fit as discussed above (Fig. 3a). The constant ^{14}CH$_4$/^{14}CO production ratio for the muon mechanisms discussed above provides an additional constraint for $P_{\mu-}^0$ and $P_{\mu f}^0$ for ^{14}CH$_4$. For ^{14}CH$_4$, we calculated negative muon capture and fast muon production rates by multiplying the corresponding ^{14}CO production rates by 0.0076 ± 0.0003; P_n^0 was the only completely free parameter in the ^{14}CH$_4$ curve fit. All the ^{14}CH$_4$ and ^{14}CO data points are fitted within the 1 σ uncertainties (Fig. 3). The curve fitting approach for ^{14}CO$_2$ was the same as for ^{14}CO.

^{14}C production from ^{16}O in quartz by fast muons has been shown in laboratory irradiation experiments (Heisinger et al., 2002a). However, to the best of our knowledge, the fast muon mechanism has never been unambiguously confirmed in a natural setting (ice or rock). Recent ^{14}C results from a 15 m deep rock core at Leymon High, Spain, suggested no significant ^{14}C production by the fast muon mechanism (Lupker et al., 2015). However, there was low confidence in this particular conclusion, owing mainly to analytical uncertainties that were as large as the ^{14}C signal for the deepest samples. We specifically tested for the presence of ^{14}C from the fast muon mechanism by attempting to fit our most complete data set (^{14}CO) with only the neutron and negative muon capture mechanisms (Fig. 3a). As can be seen, such a curve fit fails to match the observations, confirming that the fast muon mechanism is significant. Our results thus provide the first unambiguous confirmation of ^{14}C production from ^{16}O by fast muons in a natural setting.

Surface production rates for all mechanisms, scaled to sea level and high latitude using the scaling of Lifton et al. (2014) are shown in Table 7. Our results yield useful constraints for $P_{\mu f}^0$ (25% relative uncertainty) and $P_{\mu-}^0$ (29%) for ^{14}CO and ^{14}CH$_4$. For $P_{\mu f}^0$, the uncertainty in the depth of long-term ice transport provides the single largest contribution to the error. For $P_{\mu-}^0$, the curve-fitting procedure itself (which takes into account data uncertainties) and the ablation rate uncertainty are the largest sources of error. Constraints on P_n^0 are weaker due to a relatively small contribution from this mechanism (88% relative uncertainty for ^{14}CO and 47% for ^{14}CH$_4$).

We place low confidence in the production rate estimates for $^{14}CO_2$ because of the large amount of scatter in those data as well as the unknown and likely variable extraneous ^{14}C component introduced by the melt-extraction. If we make the speculative assumption that the ^{14}C content of added extraneous inorganic carbon (which affects $^{14}CO_2$) is approximately uniform across all our samples, then we could conclude that $^{14}CO_2$ is the dominant species produced by all mechanisms. This conclusion would be consistent with a prior study that was done by dry-extraction and included procedural blank characterization at another Antarctic ablation area with similar ice ^{14}C content (van der Kemp et al., 2002).

Given the large uncertainties in $^{14}CO_2$ determinations, we cannot place strong constraints on the total ^{14}C production rates. Further, experiments involving laboratory irradiation of ice suggest that non-negligible amounts of simple compounds other than $^{14}CO_2$, ^{14}CO and $^{14}CH_4$ may also be formed (e.g., Rossler et al., 1984). Our measured set of species thus may not be capable of fully characterizing the in situ cosmogenic ^{14}C. If we assume that the fraction of in situ ^{14}C that forms other compounds is relatively small, our data (Fig. 3d and Table 6) do suggest that the total ^{14}C production rates in ice commonly used in the literature (Tables 1 and 7) are overestimated.

As we now have data-based estimates of ^{14}C production rates, we are able to test our earlier assumption (Section 4.2) that in-situ cosmogenic ^{14}C inherited from the ice accumulation zone is insignificant. A detailed discussion is presented in the Electronic Annex. For ^{14}CO, we find that, at the upper limit, inherited ^{14}C represents 5% or less of measured values. This value is smaller than several other sources of uncertainty involved in the interpretation (depth of long-term ice transport, long-term ablation rate, curve fitting); neglecting this small possible contribution is therefore acceptable.

4.5. Comparison with the Scharffenbergbotnen ice ablation site

We compare our results with ^{14}CO and $^{14}CO_2$ data from a prior study at the Scharffenbergbotnen ice ablation area in Antarctica (74°34.67′ S, 11°02.97′ W, 1173 m asl) (van der Kemp et al., 2002). We consider these to be the most reliable prior determinations of ^{14}CO and $^{14}CO_2$ in ablating ice, as a dry-extraction method was used (avoiding the problematic melt-acidify approach of many other prior studies) and the study included procedural blank characterization. To perform the comparison, we attempted to fit the Scharffenbergbotnen data with the same approach we applied to our data. However, we constrained the ^{14}CO and $^{14}CO_2$ surface production rates for each mechanism to be within the uncertainties of those determined from the Taylor Glacier ^{14}C data. The value for P_n^0 was scaled by a factor of 1.80 with respect to Taylor Glacier, the value for $P_{\mu-}^0$ by a factor of 1.45 and the value for $P_{\mu f}^0$ with a factor of 1.18 (as per Lifton et al. (2014)) to account for the higher elevation of Scharffenbergbotnen. Ablation rate was adjusted to 0.16 m a^{-1} (van der Kemp et al., 2002).

Scharffenbergbotnen ice has a relatively younger age (van der Kemp et al., 2002) and is expected to have a non-negligible ^{14}C component inherited from the accumulation zone. Further, the van der Kemp et al. (2002) study did not include a correction for ^{14}C production during storage and transport of the ice. To account for these ^{14}C components, we treat D in Eq. (4) as an additional free parameter.

Fig. 5 shows the results of the curve fits. Scharffenbotnen ^{14}C results are reproduced well with ^{14}C production rates determined at Taylor Glacier, even without allowing for any uncertainty in the Scharffenbergbotnen ablation rate. This agreement is encouraging and suggests that all in situ cosmogenic ^{14}C migrates from the ice lattice into the air bubbles relatively rapidly, allowing for the

Table 6
Comparison of upper limit of total ^{14}C in sampled ice based on measurements with expected values based on production rates from prior studies as in Table 1.

Sample mid-depth, m	Upper limit of total ^{14}C, atoms/g ice	Expected total ^{14}C, atoms/g ice	Upper limit measured/expected
2.26	443 ± 24	828 ± 136	0.53 ± 0.09
3.77	338 ± 17	727 ± 132	0.47 ± 0.09
5.27	324 ± 16	662 ± 128	0.49 ± 0.10
6.77	342 ± 17	614 ± 125	0.56 ± 0.12
10.02	324 ± 16	536 ± 118	0.60 ± 0.14
15.01	207 ± 10	448 ± 110	0.46 ± 0.12
19.53	244 ± 12	390 ± 104	0.62 ± 0.17

Table 7
In situ cosmogenic ^{14}C production rates by the individual mechanisms at the ice surface as determined from Taylor Glacier data by curve fitting (Section 4.4 and Fig. 3), scaled to sea level and high latitude. All production rates are in atoms of ^{14}C g^{-1} a^{-1}. The values for $^{14}CO_2$ and total production rates are less certain, as discussed in the text. Typical total ^{14}C production values given in prior studies (same as in Table 1) are also shown for comparison.

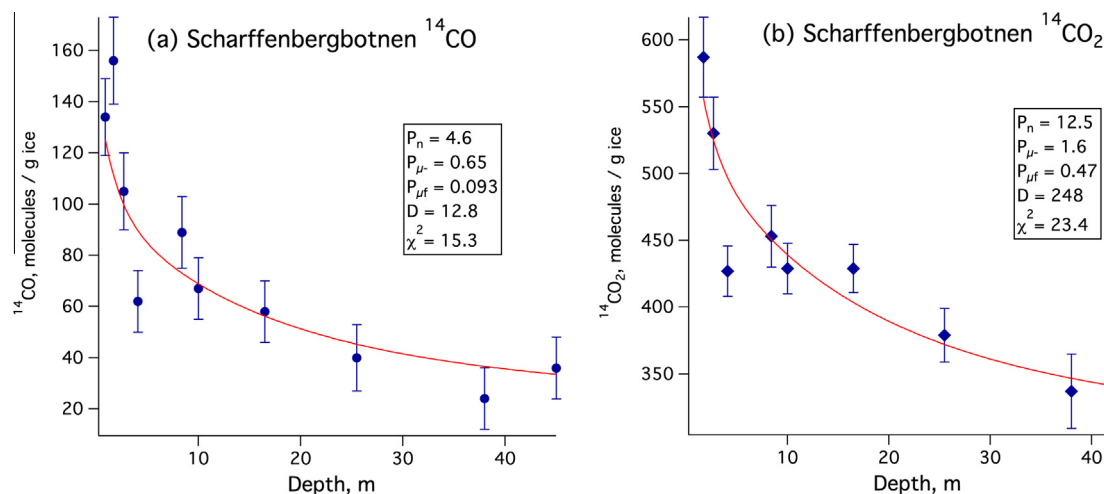|	^{14}CO	$^{14}CH_4$	$^{14}CO_2$	Total	Total, prior studies
Neutrons	0.69 ± 0.61	0.024 ± 0.011	*13.6 ± 10.1*	*14.3 ± 10.1*	20.0 ± 1.5
Muon capture	0.24 ± 0.07	0.0018 ± 0.0005	*1.5 ± 0.7*	*1.7 ± 0.7*	4.75 ± 0.4
Fast muons	0.053 ± 0.014	0.00040 ± 0.00010	*0.51 ± 0.17*	*0.56 ± 0.17*	0.74 ± 0.4

Fig. 5. Scharffenbergbotnen data from van der Kemp et al. (2002) and fit curves generated using production rates constrained by Taylor Glacier data. Production rate estimates shown are determined by the curve fit (within bounds allowed by Taylor Glacier results) and are for Scharffenbergbotnen ice surface, in ^{14}C atoms g^{-1} a^{-1}.

dry-extraction method used in the van der Kemp et al. (2002) study to quantitatively recover the ^{14}CO and ^{14}CO$_2$.

5. CONCLUSIONS AND FUTURE OUTLOOK

In this study, in situ cosmogenic production of ^{14}CH$_4$ in ice has been corroborated, and ^{14}CH$_4$ production rates have been constrained in the 2.26–19.53 m depth range of the Taylor Glacier samples. ^{14}CO measurements have improved substantially over prior work, resulting in much less scatter in the data. As a result, ^{14}CO production rates have also been successfully constrained at Taylor Glacier and appear consistent with independent data from Scharffenbergbotnen. This agreement between results from melt-extraction and dry extraction approaches suggests that in situ cosmogenic ^{14}CO is released rapidly from the ice grains into the air bubbles in the ice. This study has also provided the first confirmation of in situ cosmogenic ^{14}C production from ^{16}O by the fast muon mechanism in a natural setting.

Taylor Glacier results revealed that the ^{14}CH$_4$/^{14}CO production ratio is the same (0.0076 ± 0.0003) for the two muon mechanisms and is independent of depth. A higher ^{14}CH$_4$/^{14}CO production ratio inferred for the neutron mechanism is qualitatively consistent with earlier results from Summit, Greenland firn. The constant ^{14}CH$_4$/^{14}CO production ratio for the muon mechanisms means that ^{14}CO can be used to correct ^{14}CH$_4$ measurements for the in situ cosmogenic component in ice with negligible neutron-produced ^{14}CH$_4$. This means that it should be possible to retrieve the paleoatmospheric ^{14}CH$_4$ signal from Taylor Glacier ice deeper than ≈6 m, allowing for reliable reconstructions of the fossil fraction of the past methane budget, including testing the hypotheses of major atmospheric methane releases from methane clathrates and permafrost.

This study did not produce reliable constraints on ^{14}CO$_2$ production rates because of complications associated with the melt-extraction approach. ^{14}CO$_2$ production rates and total ^{14}C production rates in ice thus remain to be experimentally verified.

Ongoing work involves the construction of a system capable of extracting CO$_2$ from ≈1.5 kg of ice by sublimation. This approach would allow for complete ^{14}CO$_2$ release from the ice grains without the complications of a melt extraction. Ongoing work is also attempting to extend the sampling at the ≈52 ka site at Taylor Glacier to a depth of 70 m or more, to better characterize the two muon production mechanisms, as well as collect samples from very shallow ice to improve constraints on ^{14}C production by neutrons.

ELECTRONIC ANNEX

The Electronic Annex for this article can be found at http://dx.doi.org/10.1016/j.gca.2016.01.004.

REFERENCES

Aciego S. M., Cuffey K. M., Kavanaugh J. L., Morse D. L. and Severinghaus J. P. (2007) Pleistocene ice and paleo-strain rates at Taylor Glacier, Antarctica. *Quatern. Res.* **68**, 303–313.

Ahn J. and Brook E. J. (2008) Atmospheric CO_2 and climate on millennial time scales during the last glacial period. *Science* **322**, 83–85.

Andree M., Moor E., Beer J., Oeschger H., Stauffer B., Bonani G., Hofmann H. J., Morenzoni E., Nessi M., Suter M. and Wolfli W. (1984) C-14 dating of polar ice. *Nucl. Instrum. Meth. B* **5**, 385–388.

Baggenstos D. (2015) *Taylor Glacier as an Archive of Ancient Ice for Large-volume Samples: Chronology, Gases, Dust, and Climate* (Ph.D. thesis). University of California, San Diego.

Beer J., Siegenthaler U., Bonani G., Finkel R. C., Oeschger H., Suter M. and Wolffi W. (1988) Information on past solar-activity and geomagnetism from Be-10 in the camp century ice core. *Nature* **331**, 675–679.

Bertler N. A. N., Mayewski P. A. and Carter L. (2011) Cold conditions in Antarctica during the Little Ice Age – implications for abrupt climate change mechanisms. *Earth Planet. Sci. Lett.* **308**, 41–51.

Bliss A. K., Cuffey K. M. and Kavanaugh J. L. (2011) Sublimation and surface energy budget of Taylor Glacier, Antarctica. *J. Glaciol.* **57**, 684–696.

Brenninkmeijer C. A. M. (1993) Measurement of the abundance of (CO)-C-14 in the atmosphere and the C-13 C-12 and O-18 O-16 ratio of atmospheric CO with applications in New-Zealand and Antarctica. *J. Geophys. Res. Atmos.* **98**, 10595–10614.

Brook E. J., White J. W. C., Schilla A. S. M., Bender M. L., Barnett B., Severinghaus J. P., Taylor K. C., Alley R. B. and Steig E. J. (2005) Timing of millennial-scale climate change at Siple Dome, West Antarctica, during the last glacial period. *Quatern. Sci. Rev.* **24**, 1333–1343.

Buizert C., Petrenko V. V., Kavanaugh J. L., Cuffey K. M., Lifton N. A., Brook E. J. and Severinghaus J. P. (2012) In situ cosmogenic radiocarbon production and 2-D ice flow line modeling for an Antarctic blue ice area. *J. Geophys. Res.* **117**, F02029. http://dx.doi.org/10.1029/2011JF002086.

Buizert C. (2013) Studies of firn air. In *The Encyclopedia of Quaternary Science 2* (ed. S. A. Elias). Elsevier, Amsterdam, pp. 361–372.

Buizert C., Baggenstos D., Jiang W., Purtschert R., Petrenko V. V., Lu Z. T., Muller P., Kuhl T., Lee J., Severinghaus J. P. and Brook E. J. (2014) Radiometric Kr-81 dating identifies 120,000-year-old ice at Taylor Glacier, Antarctica. *Proc. Nat. Acad. Sci. U.S.A.* **111**, 6876–6881.

Buizert C., Cuffey K. M., Severinghaus J. P., Baggenstos D., Fudge T. J., Steig E. J., Markle B. R., Winstrup M., Rhodes R. H., Brook E. J., Sowers T. A., Clow G. D., Cheng H., Edwards R. L., Sigl M., McConnell J. R. and Taylor K. C. (2015) The WAIS divide deep ice core WD2014 chronology. Part 1. Methane synchronization (68–31 kaBP) and the gas age-ice age difference. *Clim. Past* **11**, 153–173.

Cunnold D. M., Steele L. P., Fraser P. J., Simmonds P. G., Prinn R. G., Weiss R. F., Porter L. W., O'Doherty S., Langenfelds R. L., Krummel P. B., Wang H. J., Emmons L., Tie X. X. and Dlugokencky E. J. (2002) In situ measurements of atmospheric methane at GAGE/AGAGE sites during 1985–2000 and resulting source inferences. *J. Geophys. Res. Atmos.* **107**(D14), 4225. http://dx.doi.org/10.1029/D001226.

de Jong A. F. M., Alderliesten C., van der Borg K., van der Veen C. and van De Wal R. S. W. (2004) Radiocarbon analysis of the EPICA Dome C ice core: no in situ C-14 from the firn observed. *Nucl. Instrum. Meth. B* **223–24**, 516–520.

Ferretti D. F., Miller J. B., White J. W. C., Etheridge D. M., Lassey K. R., Lowe D. C., Meure C. M. M., Dreier M. F., Trudinger C. M., van Ommen T. D. and Langenfelds R. L. (2005) Unexpected changes to the global methane budget over the past 2000 years. *Science* **309**, 1714–1717.

Field C. V., Schmidt G. A., Koch D. and Salyk C. (2006) Modeling production and climate-related impacts on Be-10 concentration in ice cores. *J. Geophys. Res. Atmos.* **111**, D15107. http://dx.doi.org/10.1029/2005JD006410.

Fink D., Hotchkis M., Hua Q., Jacobsen G., Smith A. M., Zoppi U., Child D., Mifsud C., van der Gaast H., Williams A. and Williams M. (2004) The ANTARES AMS facility at ANSTO. *Nucl. Instrum. Meth. B* **223–24**, 109–115.

Heisinger B., Lal D., Jull A. J. T., Kubik P., Ivy-Ochs S., Knie K. and Nolte E. (2002a) Production of selected cosmogenic radionuclides by muons. 2. Capture of negative muons. *Earth Planet. Sci. Lett.* **200**, 357–369.

Heisinger B., Lal D., Jull A. J. T., Kubik P., Ivy-Ochs S., Neumaier S., Knie K., Lazarev V. and Nolte E. (2002b) Production of selected cosmogenic radionuclides by muons 1. Fast muons. *Earth Planet. Sci. Lett.* **200**, 345–355.

Herron M. M. and Langway C. C. (1980) Firn densification – an empirical model. *J. Glaciol.* **25**, 373–385.

Hippe K. and Lifton N. A. (2014) Calculating isotope ratios and nuclide concentrations for in situ cosmogenic C-14 analyses. *Radiocarbon* **56**, 1167–1174.

Hua Q., Zoppi U., Williams A. A. and Smith A. M. (2004) Small-mass AMS radiocarbon analysis at ANTARES. *Nucl. Instrum. Meth. B* **223–24**, 284–292.

Jull A. J. T., Lal D., Donahue D. J., Mayewski P., Lorius C., Raynaud D. and Petit J. R. (1994) Measurements of cosmic-ray-produced C-14 in firn and ice from Antarctica. *Nucl. Instrum. Meth. B* **92**, 326–330.

Kavanaugh J. L. and Cuffey K. M. (2009) Dynamics and mass balance of Taylor Glacier, Antarctica. 2. Force balance and longitudinal coupling. *J. Geophys. Res.* **114**, F04011. http://dx.doi.org/10.1029/2009JF001329.

Kavanaugh J. L., Cuffey K. M., Morse D. L., Bliss A. K. and Aciego S. M. (2009a) Dynamics and mass balance of Taylor Glacier, Antarctica. 3. State of mass balance. *J. Geophys. Res.* **114**, F04012. http://dx.doi.org/10.1029/2009JF001331.

Kavanaugh J. L., Cuffey K. M., Morse D. L., Conway H. and Rignot E. (2009b) Dynamics and mass balance of Taylor Glacier, Antarctica. 1. Geometry and surface velocities. *J. Geophys. Res.* **114**, F04010. http://dx.doi.org/10.1029/2009JF001309.

Kennett J. P., Cannariato K. G., Hendy I. L. and Behl R. J. (2000) Carbon isotopic evidence for methane hydrate instability during quaternary interstadials. *Science* **288**, 128–133.

Knudsen M. F., Riisager P., Jacobsen B. H., Muscheler R., Snowball I. and Seidenkrantz M. S. (2009) Taking the pulse of the Sun during the Holocene by joint analysis of (14)C and (10) Be. *Geophys. Res. Lett.* **36**, L16701. http://dx.doi.org/10.1029/2009GL039439.

Kuhl T. W., Johnson J. A., Shturmakov A. J., Goetz J. J., Gibson C. J. and Lebar D. A. (2014) A new large-diameter ice-core drill: the Blue Ice Drill. *Ann. Glaciol.* **55**, 1–6.

Lal D., Nishiizumi K. and Arnold J. R. (1987) In situ cosmogenic H-3, C-14, and Be-10 for determining the net accumulation and ablation rates of ice sheets. *J. Geophys. Res. Solid Earth* **92**, 4947–4952.

Lal D., Jull A. J. T., Donahue D. J., Burtner D. and Nishiizumi K. (1990) Polar ice ablation rates measured using in situ cosmogenic C-14. *Nature* **346**, 350–352.

Lal D., Jull A. J. T., Burr G. S. and Donahue D. J. (1997) Measurements of in situ C-14 concentrations in Greenland Ice Sheet Project 2 ice covering a 17-kyr time span: implications to ice flow dynamics. *J. Geophys. Res.* **102**, 26505–26510.

Lal D., Jull A. J. T., Burr G. S. and Donahue D. J. (2000) On the characteristics of cosmogenic in situ C-14 in some GISP2

Holocene and late glacial ice samples. *Nucl. Instrum. Meth. B* **172**, 623–631.

Lal D., Jull A. J. T., Donahue D. J., Burr G. S., Deck B., Jouzel J. and Steig E. (2001) Record of cosmogenic in situ produced C-14 in Vostok and Taylor Dome ice samples: implications for strong role of wind ventilation processes. *J. Geophys. Res. Atmos.* **106**, 31933–31941.

Lal D., Jull A. J. T., Pollard D. and Vacher L. (2005) Evidence for large century time-scale changes in solar activity in the past 32 Kyr, based on in-situ cosmogenic C-14 in ice at Summit, Greenland. *Earth Planet. Sci. Lett.* **234**, 335–349.

Leuker T. J. (1998) *The Ratio of the First and Second Dissociation Constants of Carbonic Acid Determined from the Concentration of Carbon Dioxide in Gas and Seawater at Equilibrium* (Ph.D. thesis). University of California, San Diego.

Lifton N., Sato T. and Dunai T. J. (2014) Scaling in situ cosmogenic nuclide production rates using analytical approximations to atmospheric cosmic-ray fluxes. *Earth Planet. Sci. Lett.* **386**, 149–160.

Lowe D. C., Brenninkmeijer C. A. M., Tyler S. C. and Dlugkencky E. J. (1991) Determination of the isotopic composition of atmospheric methane and its application in the Antarctic. *J. Geophys. Res. Atmos.* **96**, 15455–15467.

Lupker M., Hippe K., Wacker L., Kober F., Maden C., Braucher R., Bourles D., Romani J. R. V. and Wieler R. (2015) Depth-dependence of the production rate of in situ C-14 in quartz from the Leymon High core, Spain. *Quatern. Geochronol.* **28**, 80–87.

Masarik J. and Beer J. (1999) Simulation of particle fluxes and cosmogenic nuclide production in the Earth's atmosphere. *J. Geophys. Res. Atmos.* **104**, 12099–12111.

Mitchell L., Brook E., Lee J. E., Buizert C. and Sowers T. (2013) Constraints on the late Holocene anthropogenic contribution to the atmospheric methane budget. *Science* **342**, 964–966.

Mühle J., Lueker T. J., Su Y., Miller B. R., Prather K. A. and Weiss R. F. (2007) Trace gas and particulate emissions from the 2003 southern California wildfires. *J. Geophys. Res. Atmos.* **112**, D03307. http://dx.doi.org/10.1029/2006JD007350.

Muscheler R., Joos F., Beer J., Muller S. A., Vonmoos M. and Snowball I. (2007) Solar activity during the last 1000 yr inferred from radionuclide records. *Quatern. Sci. Rev.* **26**, 82–97.

National Climatic Data Center (2015). <www.ncdc.noaa.gov> (data accessed September 2015).

Nesterenok A. and Naidenov V. (2012) In situ formation of cosmogenic C-14 by cosmic ray nucleons in polar ice. *Nucl. Instrum. Meth. B* **270**, 12–18.

O'Connor F. M., Boucher O., Gedney N., Jones C. D., Folberth G. A., Coppell R., Friedlingstein P., Collins W. J., Chappellaz J., Ridley J. and Johnson C. E. (2010) Possible role of wetlands, permafrost, and methane hydrates in the methane cycle under future climate change: a review. *Rev. Geophys.* **48**, RG4005. http://dx.doi.org/10.1029/2010RG000326.

Petrenko V. V., Severinghaus J. P., Brook E. J., Mühle J., Headly M., Harth C., Schaefer H., Reeh N., Weiss R., Lowe D. C. and Smith A. M. (2008a) A novel method for obtaining very large ancient air samples from ablating glacial ice for analyses of methane radiocarbon. *J. Glaciol.* **54**, 233–244.

Petrenko V. V., Smith A. M., Brailsford G., Riedel K., Hua Q., Lowe D., Severinghaus J. P., Levchenko V., Bromley T., Moss R., Muhle J. and Brook E. J. (2008b) A new method for analyzing C-14 of methane in ancient air extracted from glacial ice. *Radiocarbon* **50**, 53–73.

Petrenko V. V., Smith A. M., Brook E. J., Lowe D., Riedel K., Brailsford G., Hua Q., Schaefer H., Reeh N., Weiss R. F., Etheridge D. and Severinghaus J. P. (2009) (CH4)-C-14 measurements in Greenland ice: investigating last glacial termination CH4 sources. *Science* **324**, 506–508.

Petrenko V. V., Severinghaus J. P., Smith A. M., Riedel K., Baggenstos D., Harth C., Orsi A., Hua Q., Franz P., Takeshita Y., Brailsford G. W., Weiss R. F., Buizert C., Dickson A. and Schaefer H. (2013) High-precision C-14 measurements demonstrate production of in situ cosmogenic (CH4)-C-14 and rapid loss of in situ cosmogenic (CO)-C-14 in shallow Greenland firn. *Earth Planet. Sci. Lett.* **365**, 190–197.

Rhodes R. H., Bertler N. A. N., Baker J. A., Steen-Larsen H. C., Sneed S. B., Morgenstern U. and Johnsen S. J. (2012) Little Ice Age climate and oceanic conditions of the Ross Sea, Antarctica from a coastal ice core record. *Clim. Past* **8**, 1223–1238.

Rossler K., Jung H. J. and Nebeling B. (1984) Hot atoms in cosmic chemistry. *Adv. Space Res.* **4**, 83–95.

Schmitt J., Seth B., Bock M., van der Veen C., Moller L., Sapart C. J., Prokopiou M., Sowers T., Rockmann T. and Fischer H. (2013) On the interference of Kr during carbon isotope analysis of methane using continuous-flow combustion-isotope ratio mass spectrometry. *Atmos. Meas. Tech.* **6**, 1425–1445.

Schwander J., Stauffer B. and Sigg A. (1988) Air mixing in firn and the age of the air at pore close-off. *Ann. Glaciol.* **10**, 141–145.

Schwander J., Barnola J. M., Andrie C., Leuenberger M., Ludin A., Raynaud D. and Stauffer B. (1993) The age of the air in the firn and the ice at Summit, Greenland. *J. Geophys. Res. Atmos.* **98**, 2831–2838.

Severinghaus J. P., Beaudette R., Headly M. A., Taylor K. and Brook E. J. (2009) Oxygen-18 of O(2) records the impact of abrupt climate change on the terrestrial biosphere. *Science* **324**, 1431–1434.

Smith A. M., Levchenko V. A., Etheridge D. M., Lowe D. C., Hua Q., Trudinger C. M., Zoppi U. and Elcheikh A. (2000) In search of in-situ radiocarbon in Law Dome ice and firn. *Nucl. Instrum. Meth. B* **172**, 610–622.

Steig E. J., Morse D. L., Waddington E. D., Stuiver M., Grootes P. M., Mayewski P. A., Twickler M. S. and Whitlow S. I. (2000) Wisconsinan and Holocene climate history from an ice core at Taylor Dome, western Ross Embayment, Antarctica. *Geograf. Ann.* **82A**, 213–235.

Steinhilber F., Beer J. and Frohlich C. (2009) Total solar irradiance during the Holocene. *Geophys. Res. Lett.* **36**(L19704), 2009G. http://dx.doi.org/10.1029/L040142.

Stuiver M. and Polach H. A. (1977) Reporting of C-14 data – discussion. *Radiocarbon* **19**, 355–363.

van de Wal R. S. W., van der Borg K., Oerter H., Reeh N., De Jong A. F. M. and Oerlemans J. (1990) Progress in carbon-14 dating of ice at Utrecht. *Nucl. Instrum. Meth. B* **52**, 469–472.

van de Wal R. S. W., Meijer H. A. J., de Rooij M. and van der Veen C. (2007) Radiocarbon analyses along the EDML ice core in Antarctica. *Tellus B* **59**, 157–165.

van der Kemp W. J. M., Alderliesten C., van der Borg K., Holmlund P., de Jong A. F. M., Karlof L., Lamers R. A. N., Oerlemans J., Thomassen M. and van de Wal R. S. W. (2000) Very little in situ produced radiocarbon retained in accumulating Antarctic ice. *Nucl. Instrum. Meth. B* **172**, 632–636.

van der Kemp W. J. M., Alderliesten C., van der Borg K., de Jong A. F. M., Lamers R. A. N., Oerlemans J., Thomassen M. and van de Wal R. S. W. (2002) In situ produced C-14 by cosmic ray muons in ablating Antarctic ice. *Tellus B* **54**, 186–192.

van Roijen J., van der Borg K., DeJong A. and Oerlemans J. (1995) A correction for in-situ C-14 in Antarctic ice with (CO)-C-14. *Radiocarbon* **37**, 165–169.

Yang B., Smith A. M. and Hua Q. (2013) A cold finger cooling system for the efficient graphitisation of microgram-sized carbon samples. *Nucl. Instrum. Meth. B* **294**, 262–265.

Young N. E., Schaefer J. M., Goehring B., Lifton N., Schim-melpfennig I. and Briner J. P. (2014) West Greenland and global in situ C-14 production-rate calibrations. *J. Quatern. Sci.* **29**, 401–406.

WAIS Divide Project Members (2015) Precise interpolar phasing of abrupt climate change during the last ice age. *Nature* **520**, 661–665.

Walter K. M., Edwards M. E., Grosse G., Zimov S. A. and Chapin, III, F. S. (2007a) Thermokarst lakes as a source of atmospheric CH_4 during the last deglaciation. *Science* **318**, 633–636.

Walter K. M., Smith L. C. and Chapin F. S. (2007b) Methane bubbling from northern lakes: present and future contributions to the global methane budget. *Phil. Trans. R. Soc. A* **365**, 1657–1676.

Associate editor: Thure E. Cerling